ELSEVIER

Ultrasonics 36 (1998) 349–353

Ultrasonics

Surface dynamic response functions of anisotropic solids

A.G. Every [a,*], K.Y. Kim [b], A.A. Maznev [c]

[a] *Department of Physics, University of the Witwatersrand, PO WITS 2050, Johannesburg, South Africa*
[b] *Department of Theoretical and Applied Mechanics, Cornell University, Ithaca, NY 14853, USA*
[c] *Department of Chemistry, MIT, Cambridge, MA 02139, USA*

Abstract

An integral expression is established for the surface displacement response tensor of a semi-infinite anisotropic elastic continuum to sudden loading at a point on the surface. The expression is numerically evaluated for normal force and displacement in a number of directions in the Cu (001) surface, and the results compared with waveforms measured in a copper single crystal. The predicted singularities associated with bulk and surface wave arrivals are clearly observed. Because of folding of the Rayleigh wave group velocity curve, there are multiple surface wave arrivals in some directions. Near the [110] direction the response is dominated by a pseudo surface wave resonance. © 1998 Elsevier Science B.V.

Keywords: Anisotropy; Dynamic response; Green's function

1. Introduction

The elastodynamic response functions of solids find application in many areas of science, including materials characterization, non-destructive testing and seismology. Over the years considerable effort has been devoted to calculating these functions for solids of various types (isotropic, anisotropic, viscoelastic) and geometries (infinite continuum, halfspace, plate geometry). The methods for treating isotropic solids are well established, and are described in a number of books on the dynamics of solids [1–3]. The growing technological importance of anisotropic materials and the recognition of the important role of anisotropy in seismology have focused attention on the elasodynamics of anisotropic solids. The response of an anisotropic half-space to an impulsive line load has been obtained by Burridge [4] using the Cagniard method, and Maznev and Every [5] have derived a similar result by Fourier transformation. Willis [6] in a seminal paper has obtained the formal solution to a wide class of self-similar problems for the anisotropic half-space using Fourier and radon transforms, and this method has been further developed by Wang and Achenbach [7]. Recently Mourad at al. [8] have used the Cagniard de Hoop method to calculate the interior response of anisotropic halfspaces of hexagonal and cubic symmetry to point loading, and Tewary and Fortunko [9] have treated the same problem by integral representation in terms of a δ function.

In this paper we calculate the surface displacement response of a semi-infinite anisotropic elastic continuum to sudden loading at a point on the surface. Our approach is to Fourier transform the equations of motion and boundary conditions with respect to time and the spatial coordinates parallel to the surface, solve the resulting algebraic equations, and then carry out the inverse transform. Analytical means are then used to reduce the surface response to a one-dimensional integral for numerical evaluation. The method is readily implemented computationally, and we present calculated responses for the Cu(001) surface that are in good agreement with waveforms we have measured in a (001) oriented copper single crystal using capillary fracture generation and capacitive detection.

2. Method of calculation

As full details of our method of calculation are published elsewhere [10], only a brief outline is given here. We consider a general anisotropic elastic continuum of density ρ and elastic modulus tensor C_{ijkl} occupying the half-space $x_3>0$. A concentrated point

* Corresponding author. Fax: +27 11 339 8262;
e-mail: every@physnet.phys.wits.ac.za

PII S0041-624X(97)00039-5

force $\mathbf{F}(t)=(F_j\Theta(t))$ with Heaviside step-function time dependence $\Theta(t)$ acts at the origin on the otherwise free surface of the half-space. The displacement field in response to this force, $u_i(\mathbf{x},t)=G_{ij}(\mathbf{x},t)F_j$, where $G_{ij}(\mathbf{x},t)$ is the response function tensor, satisfies the equations of motion

$$\rho\frac{\partial^2 u_i}{\partial t^2}=C_{ijkl}\frac{\partial^2 u_l}{\partial x_j\partial x_k},\quad x_3>0, \tag{1}$$

subject to the boundary conditions on the stress tensor:

$$\sigma_{l3}(\mathbf{x}_\parallel,x_3=0_+,t)=F_j\delta_{jl}\delta(\mathbf{x}_\parallel)\epsilon(t), \tag{2}$$

where $\mathbf{x}_\parallel=(x_1,x_2)$ denotes the position vector in the surface and $\delta(\mathbf{x}_\parallel)=\delta(x_1)\delta(x_2)$ is the two-dimensional δ-function.

We seek a solution to the above equations of motion and boundary conditions in the form of a superposition of outgoing plane waves whose amplitudes are proportional to F_j:

$$u_i(\mathbf{x},t)=\int_{-\infty}^{\infty}\mathrm{d}^2k_\parallel\int_{-\infty}^{\infty}\mathrm{d}\omega\sum_{n=1}^{3}A_j^{(n)}F_jU_i^{(n)}\times\exp\{i(\mathbf{k}_\parallel.\mathbf{x}_\parallel+k_3^{(n)}x_3-wt)\}+\text{const.} \tag{3}$$

For each value of the angular frequency ω and wavevector $\mathbf{k}_\parallel=\omega\mathbf{s}_\parallel$, where $\mathbf{s}=\mathbf{k}/\omega$, is the acoustic slowness vector, the third component $k_3=\omega s_3$ and the polarization vector $\mathbf{U}$ are related by the Christoffel equations

$$(C_{ijkl}s_js_k-\rho\delta_{il})U_l=0, \tag{4}$$

and $s_3^{(n)}$ are roots of the secular equation

$$\det|C_{ijkl}s_js_k-\rho\delta_{il}|=0. \tag{5}$$

Eq. (5) yields six solutions of which only the three corresponding to outgoing waves, i.e. homogeneous (bulk) waves with ray vectors directed into the interior, or inhomogeneous (evanescent) waves which decay into the interior, are retained. The stress–strain relationship, $\sigma_{lm}=C_{lmpq}\partial u_p/\partial x_q$ together with Eqs. (2) and (3) yield a set of linear equations that determine the partial wave amplitudes $A_j^{(n)}$ and thereby $\mathbf{u}(\mathbf{x},t)$. We obtain the surface response by taking the observation point $\mathbf{x}$ to be along the x_1-axis, with $x_2=x_3=0$. The integration with respect to ω in Eq. (3) can be performed analytically, yielding

$$G_{ij}(x_1,t)=-\frac{1}{4\pi^3}\left[-\mathscr{P}\int_{-\infty}^{+\infty}\mathrm{d}s_1\frac{\mathrm{Im}\Phi_{ij}(s_1)}{(s_1x_1-t)}+\frac{\pi}{|x_1|}\mathrm{Re}\,\Phi_{ij}(t/x_1)\right]+\text{const.}, \tag{6}$$

where

$$\Phi_{ij}(s_1)=\int_{-\infty}^{\infty}\mathrm{d}s_2\,\Psi_{ij}(\mathbf{s}_\parallel), \tag{7}$$

$$\Psi_{ij}(\mathbf{s}_\parallel)=\sum_{n=1}^{3}\frac{\mathrm{adj}(\mathbf{B})_j^{(n)}U_i^{(n)}}{\det|\mathbf{B}|}, \tag{8}$$

and

$$B_l^{(n)}=\sum_{pq}C_{3lpq}U_p^{(n)}s_q^{(n)} \tag{9}$$

is the boundary condition matrix.

Using the fact that for negative times $G_{ij}(x_1,t)$ is constant, we arrive at a Kramers–Kronig-type relation for Φ:

$$-\mathscr{P}\int_{-\infty}^{+\infty}\mathrm{d}s_1\frac{\mathrm{Im}\Phi_{ij}(s_1)}{s_1x_1-t}=\frac{\pi}{|x_1|}\mathrm{Re}\Phi_{ij}(t/x_1)+\text{const.}, \tag{10}$$

which disposes of the integration with respect to s_1. It follows that

$$G_{ij}(x_1,t>0)=-\frac{1}{2\pi^2|x_1|}\mathrm{Re}\{\Phi_{ij}(t/x_1)-\Phi_{ij}(0)\}. \tag{11}$$

For an isotropic solid this integral can be performed analytically, but for an anisotropic solid numerical methods are in general required for its evaluation. In all except possibly a few isolated directions of $\mathbf{s}_\parallel$, there is a single Rayleigh surface wave (RW), conditioned on the vanishing of the boundary condition determinant $\det|B(\mathbf{s}_\parallel)|$.

2.1. Numerical integration

For an anisotropic solid the integration over s_2 in Eq. (7) to obtain Φ_{ij} has in general to be done numerically. Fig. 1 shows the dependence of $\mathrm{Re}(\Psi_{33})$ on s_1 and s_2 for the Cu (001) surface as a grey-scale 'image', with degree of darkness corresponding to the magnitude of $\mathrm{Re}(\Psi_{33})$. To render the RW singularity visible, it has been artificially broadened by making the replacement

$$\Psi_{33}\to 1/(1/\Psi_{33}+\alpha), \tag{12}$$

where α is a small but finite positive number. The continuously shaded area comprises the $\mathrm{Re}(\Psi_{33})$ weighted projections $\mathbf{s}_\parallel$ of the slowness vectors of all bulk modes in the first quadrant, its outer boundary being the so-called transonic state. The lines which stand out as lighter and which partition this domain, lie on the locus of limiting slownesses for the individual branches. This locus and the transonic state are the projection on the (s_1, s_2)-plane of points on the three sheets of the slowness surface where the surface normal, which is the ray directon, is parallel to the (s_1, s_2)-plane. Along the [110] direction the ST bulk

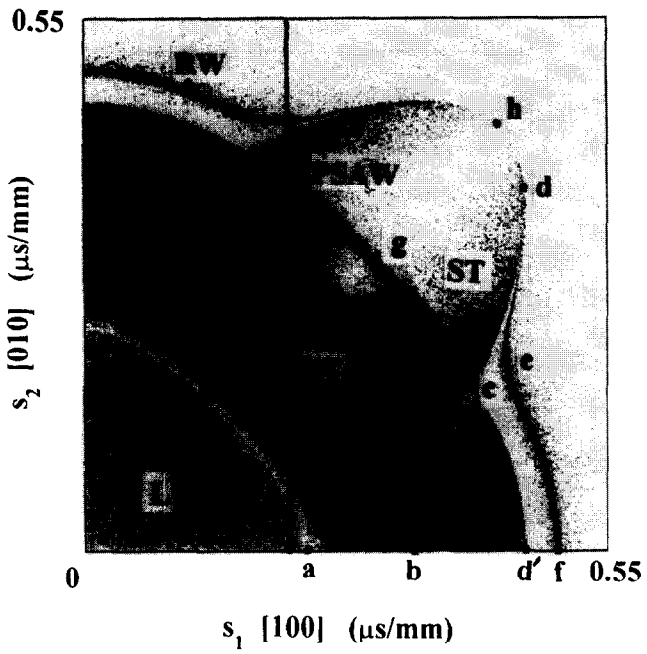

Fig. 1. Grey-scale representation of $\mathrm{Re}(\psi_{33}(s_1, s_2))$ for the Cu(001) surface.

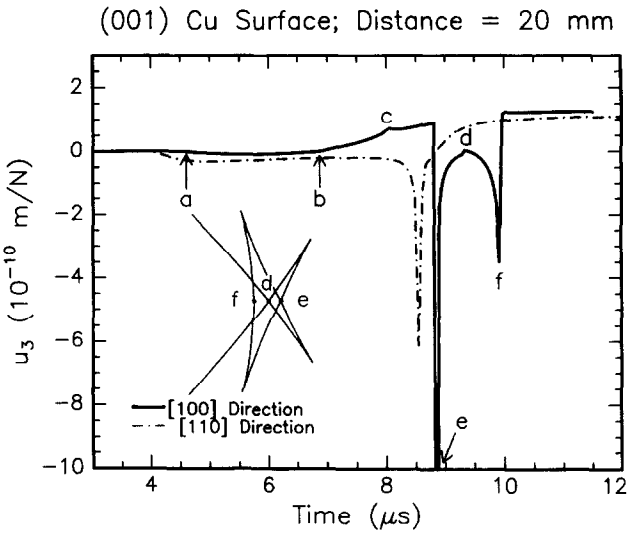

Fig. 2. Surface responses $u_3 = G_{33}(|x_1| = 20\,\mathrm{mm}, t)$ for the [100] and [110] directions in Cu (001). The insert shows portion of the RW group velocity curve near the [100] direction.

modes are SH polarized normal to the $(\bar{1}10)$ symmetry plane, and thus do not contribute to $\mathrm{Re}(\Psi_{33})$, which pertains to normal force and displacement. This is evident from the fading of the ST modes in this region of the plot. The sharp RW resonance is most intense in the [100] direction, and fades away towards the [110] direction, where it degenerates with the transonic state.

In the region extending about 20° to either side of the [110] direction there is a pseudo-surface acoustic wave (PSAW) resonance lying within the band of ST bulk modes. Exactly in the [110] direction the PSAW becomes a pure supersonic two-component SAW.

The method we have used in calculating $G_{ij}(x_1, t)$, is to make the replacement (12) and then evaluate the integral (7) numerically for 250 values of t. Over most of the range of s_2, Ψ_{ij} is slowly varying, but in isolated regions there are the sharp RW or PSAW resonances, and kinks at limiting branch slownesses to contend with. We have dealt with this problem by dividing the range of s_2 into a number of intervals and applying Rhomberg integration to each interval. It is only the few intervals where Ψ_{ij} is rapidly varying that more than one Rhomberg iteration is required to achieve convergence.

2.2. Wave arrival singularities

Fig. 2 shows the surface response function $G_{33}(|x_1| = 20\,\mathrm{mm}, t)$ calculated for the [100] direction in the Cu (001) surface (the solid line). The response is zero until the first bulk wave arrival at $t_a = 4.62$ μs, at which instant there is a sudden downward kink corresponding to a discontinuous change in velocity. This event is the longitudinal wave arrival, and is associated with the sharp dip in $\mathrm{Re}(\Psi_{33})$ at the limiting longitudinal slowness labelled 'a' in Fig. 1. The kinks in G_{33} at $t_b = 6.88$ μs and $t_c = 8.04$ μs are bulk transverse wave arrivals, and correspond to the limiting transverse slownesses labelled 'b' and 'c' in Fig. 1. These singularities propagate outwards from the point of excitation at the bulk wave group velocities in any direction. Bulk wave arrival singularities and the analytic form they take in the response functions of infinite anisotropic continua have been surveyed in Ref. [11].

At the surface there are also RW arrival singularities. These are generally much more prominent than the bulk wave arrivals. RW arrivals are conditioned by tangency

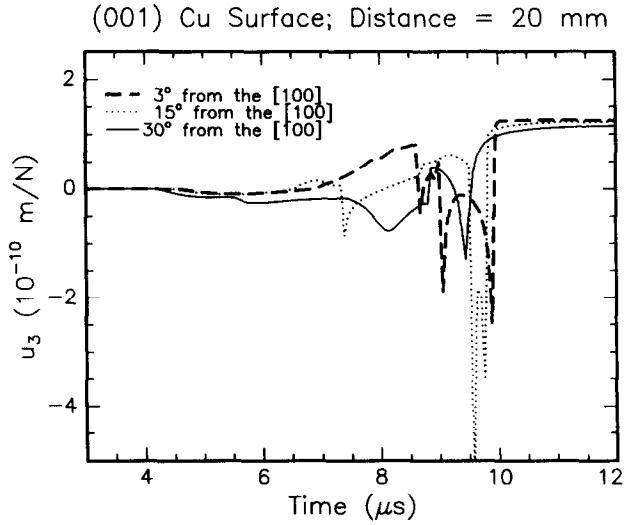

Fig. 3. Surface responses $u_3 = G_{33}(|x_1| = 20\,\mathrm{mm}, t)$ for three directions intermediate between [100] and [110] in the Cu(001) surface.

of the line $s_1 = s_R = t_R/|x_1|$ with the RW slowness curve. At the point of tangency the RW group velocity, which is normal to the RW slowness curve, is of magnitude $1/s_R$, and this is the velocity with which the wave arrival singularity propagates along the surface. The analytical form of G_{ij} for t near t_R depends on the particular ij component, whether the surface of the half-space is a materials symmetry plane or not, and whether the RW slowness curve is convex or concave at the point of tangency [10]. For a general direction, G_{ij} diverges as $1/|t_R - t|$ on either one or both sides of the wave arrival time t_R, and under certain conditions is constant after the last arrival. The sharp dips in Fig. 2 at $t_e = 8.86$ μs, and $t_f = 9.90$ μs are RW arrival singularities. Beyond t_f, G_{33} is constant, since $\mathrm{Re}(\Psi_{33})$ is zero outside the RW slowness curve. There is a third RW arrival singularity at t_d, but it is a small feature because point 'd' is close to where the RW degenerates with the transonic state and becomes SH in character.

The inset in Fig. 2 depicts the RW group velocity curve for Cu(001) near the x_1-axis, with the three rays corresponding to t_e, t_f and t_d being indicated. Ray 'e' lies at the intersection of two velocity curves, and with small deviations from [100] there is a splitting in the arrival t_e. This is evident in the response function for the direction at 3° to [100] in Fig. 3. The ray 'f', by contrast, is a singlet, and does not undergo splitting.

Also shown in Fig. 2 is the response function $G_{33}(|x_1 = 20\ \mathrm{mm}, t)$ for the [110] direction (the chain dotted line). The sharp dip at 8.6 μs is associated with a two-component supersonic SAW. The third phase-matched partial wave, which is a SH polarized bulk wave, is decoupled from the first two. For small deviations from the [110] symmetry direction the bulk partial wave component acquires a finite amplitude, and the mode becomes a PSAW. Responses in directions intermediate between [100] and [110] are shown in Fig. 3.

2.3. Comparison with experiment

We compare here the computed responses G_{33} described above with surface waveforms measured in a (001) oriented copper single crystal (see Fig. 4). These waveforms have been generated by the capillary fracture technique, which is able to simulate a suddenly applied force normal to the surface [12]. The normal displacement at a point elsewhere on the surface, in response to this force, is measured using a small aperture capacitive detector. We compare the voltage signal from the capacitive detector, which is proportional to the normal displacement of the sensed surface, with G_{33}. The data pertains to early times prior to the arrival of reflected waves from the sidewalls and opposite surface of the sample. As can be seen from a comparison of Figs. 2 and 3 with Fig. 4, the computed half-space response functions are in good agreement with the measured

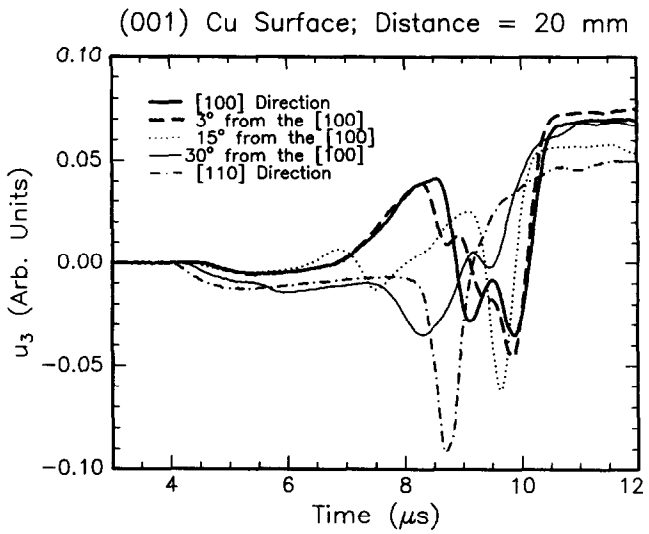

Fig. 4. Measured responses in the Cu(001) surface for the same directions as in Figs. 2 and 3. The separation between the source and detection points is 20 mm.

waveforms, particularly with regard to the bulk and surface wave arrival singularities. Naturally, because of the finite rise time of the force, which is of the order of 100 ns, the finite bandwidth of the signal processing circuitry, and the small but finite sizes of the forcing and sensing areas, there is some rounding of the measured data as compared with the computed response functions.

For the [100] direction there is a deep minimum close to the predicted RW arrival time t_f, and another at a time slightly later than the predicted RW arrival t_e. The latter slight discrepancy can be attributed to the sensitivity of the arrival e to slight misalignment of the observation direction. There are distinct features in the waveform that conform closely to the bulk wave arrivals at t_a, t_b and t_c. The splitting in the wave arrival e with change in the observation direction is clearly evident in the waveform for 3° from [100]. By 15° from [100] the first RW arrival is at 7.3 μs, which preceeds the last bulk wave arrival. There are two closely spaced RW arrivals near 9.7 μs, which are unresolved in the measured waveform, appearing as a single deep minimum. In the [110] waveform, the supersonic SAW (PSAW) and L arrival are the most prominent features, and conform closely to calculation.

References

[1] K. Aki, P. Richards, Quantitative Seismology, Freeman, San Francisco, CA, 1980.
[2] J.D. Achenbach, Wave Propagation in Elastic Solids, North-Holland, Amsterdam, 1973.
[3] A.C. Eringen, E.S. Suhubi, Elastodynamics, Academic Press, New York, 1975.
[4] R. Burridge, Quart. J. Mech. Appl. Math. 24 (1971) 81.
[5] A.A. Maznev, A.G. Every, Int. J. Engng. Sci. 35 (1997) 321.

[6] J.R. Willis, Phil. Trans. Roy. Soc. London 274 (1973) 435.
[7] C.Y. Wang, J.D. Achenbach, Wave Motion 24 (1996) 227.
[8] A. Mourad, M. Deschamps, J. Acoust. Soc. Am. 97 (1995) 3194.
[9] (a) V.K. Tewary, Phys. Rev. B 51 (1995) 15695; (b) V.K. Tewary, C.M. Fortunko, J. Acoust. Soc. Am. 100 (1996) 86.
[10] A.G. Every, K.Y. Kim, A.A. Maznev, J. Acoust. Soc. Am. 102 (1997) 1346.
[11] A.G. Every, K.Y. Kim, J. Acoust. Soc. Am. 95 (1994) 2505.
[12] K.Y. Kim, L. Niu, B. Castagnede, W. Sachse, Rev. Sci. Instrum. 60 (1989) 2785.